Detection and Tracking of Objects in Underwater Video

Dirk Walther
Computation and Neural Systems
California Institute of Technology
Pasadena, CA 91125
walther@caltech.edu

Duane R. Edgington
Monterey Bay Aquarium
Research Institute (MBARI)
Moss Landing, CA 95039
duane@mbari.org

Christof Koch
Computation and Neural Systems
California Institute of Technology
Pasadena, CA 91125
koch@klab.caltech.edu

Abstract

For oceanographic research, remotely operated underwater vehicles (ROVs) routinely record several hours of video material each day. Manual processing of such large amounts of video has become a major bottleneck for scientific research based on this data. We have developed an automated system that detects and tracks objects that are of potential interest for human video annotators. By pre-selecting salient targets for track initiation using a selective attention algorithm, we reduce the complexity of multi-target tracking, in particular of the assignment problem. Detection of low-contrast translucent targets is difficult due to variable lighting conditions and the presence of ubiquitous noise from high-contrast organic debris ("marine snow") particles. We describe the methods we developed to overcome these issues and report our results of processing ROV video data.

1. Introduction

Ocean-going remotely operated vehicles (ROVs) increasingly replace the traditional tow net approach of assessing the kinds and numbers of animals in the oceanic water column [1]. High-resolution video equipment on board the ROVs is used to obtain quantitative video transects (QVTs) through the ocean midwater, from 50 m to 1000 m depth. QVTs are superior to tow nets in assessing the spatial distribution of animals, and in recording delicate gelatinous animals that are destroyed in nets. Unlike tow nets, which integrate data over the length of the tow, QVTs provide high-resolution data at the scale of the individual animals and their natural aggregation patterns for animals and other objects larger than about 2 cm in length [2, 3, 4].

However, the current manual method of analyzing QVT video material is labor intensive and tedious. Highly trained scientists view the video tapes, annotate the animals, and enter the annotations into a data base. This method poses serious limitations to the volume of ROV data that can be analyzed, which in turn limits the length and depth increments of QVTs as well as the sampling frequency that are practical with ROVs.

Being able to process large amounts of such video data automatically would lead to an order-of-magnitude shift in (1) lateral scale of QVTs from current 0.5 km to mesoscale levels (5 km); (2) depth increment, from current 100 m to the biologically significant 10 m scale; and (3) sampling frequency, from currently monthly to daily, which is the scale of dynamic biological processes. Such an increase in data would enable modeling of the linkage between biological processes and physicochemical hydrography.

In this paper we report our progress towards such an automated system. In section 2, we describe the set of algorithms that we use as well as their integration and implementation. In section 3, we report results from comparing the performance of our system with human expert annotations, and section 4 concludes our paper.

2. Algorithms

We have developed an automated system for detecting and tracking animals visible in ROV videos. This task is difficult due to the low contrast of many of the marine animals, their sparseness in space and time, and due to debris ("marine snow") cluttering the scene, which shows up as ubiquitous high contrast clutter in the video.

Our system consists of a number of sub-components whose interactions are outlined in fig. 1. The first step for all video frames is the removal of background. Next, the first frame, and every pth frame after that (typically, $p = 5$) are processed with an attentional selection algorithm to detect salient objects. Detected objects that do not coincide with already tracked objects are used to initiate new tracks. Objects are tracked over subsequent frames, and their occurrence is verified in the proximity of the predicted location. Finally, detected objects are marked in the video frames.

2.1. Background subtraction

Images captured from the video stream often contain artefacts such as lense glare, parts of the camera housing, or parts of the ROV or instrumentation. Also, non-uniform

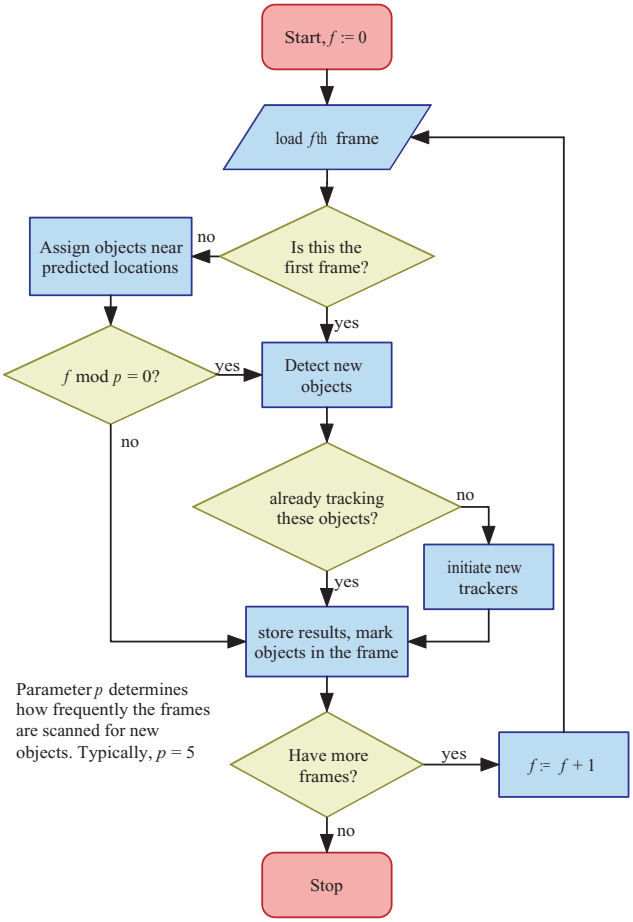

Figure 1: Interactions between the various modules of our system for detecting and tracking marine animals in underwater video.

lighting conditions cause luminance gradients that can be confusing for a contrast-based detection algorithm. All of these effects are constant over medium or long periods of time, unlike the apparently fast moving objects in the water. Hence we can remove them by background subtraction (x, y and t are assumed to be discrete):

$$I'(x,y,t) = \left[I(x,y,t) - \frac{1}{\Delta t_b} \sum_{t'=(t-\Delta t_b)}^{t-1} I(x,y,t') \right]_+ \quad (1)$$

where $I(x,y,t)$ is the intensity at image location (x,y) at time t in the original image, and I' after background subtraction. Only the non-negative part of the background subtraction is retained, symoblized by $[\cdot]_+$. This process is repeated separately for the red, green, and blue channels of the RGB color images.

The value of the time interval Δt_b for background averaging should be larger than the typical dwell time of objects at the same position in the camera plane and shorter than the

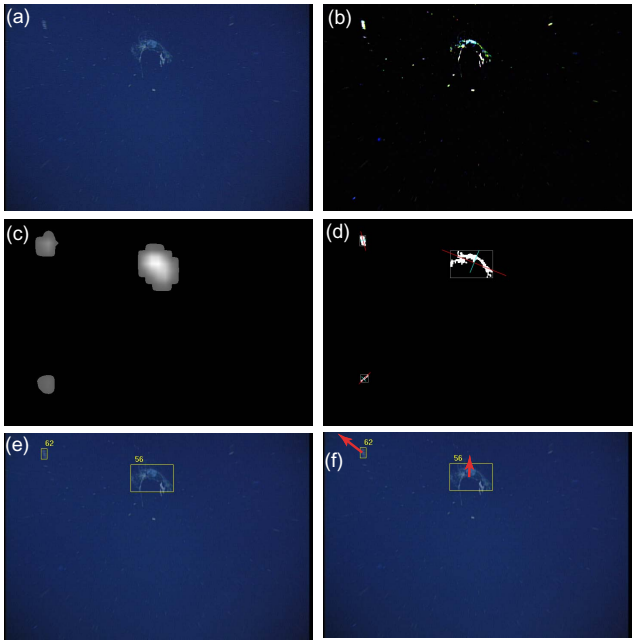

Figure 2: Processing steps for detecting objects in video frames. (a) original frame (720×480 pixels, 24 bits color depth); (b) after background subtraction according to eq. 1 (contrast enhanced for displaying purpose); (c) saliency map for the preprocessed frame (b); (d) detected objects with bounding box and major and minor axes marked; (e) the detected objects marked in the original frame and assigned to tracks – note that the small object in the lower left corner is discarded, because it was not tracked for at least five frames; (f) direction of motion of the objects obtained from eq. 11.

timescale of changes in the artefacts. In our transect videos objects typically move fast. We found that $\Delta t_b = 0.33\ s$ (10 frames) works quite well, giving us enough flexibility to adjust to changes in the artefacts quickly (fig. 2b).

2.2. Detection

For the detection of new objects we use the saliency-based bottom-up attention system by Itti & Koch [5] that has been shown to work well for a variety of applications [6, 7].

Following background subtraction, input frames are decomposed into seven channels (intensity contrast, red/green and blue/yellow double color opponencies, and the four canonical, spatial orientations) at six spatial scales, yielding 42 "feature maps". After iterative spatial competition for salience within each map, only a sparse number of locations remain active, and all maps are combined into a unique "saliency map" (fig. 2c). The saliency map is scanned by the focus of attention in order of decreasing saliency, through the interaction between a winner-take-all neural network (which selects the most salient location at any given time) and an inhibition-of-return mechanism (transiently suppressing the currently attended location from the

saliency map). Objects are segmented from the image at the salient locations, and their centroids are used to initiate tracking (see section 2.3).

We found that oriented edges are the most important feature for detecting marine animals. Many animals that are marked by human annotators have low contrast but are conspicuous due to their clearly elongated edges (fig. 3a). We compute oriented filter responses in a pyramid using steerable filters [8, 9] at four orientations. However, high-contrast "marine snow" particles that lack a preferred orientation often elicit a stronger filter response than faint string-like animals with a clear preferred orientation (fig. 3c). In order to improve the performance of the orientation filters in detecting such faint yet clearly oriented edges, we use a normalization scheme that is inspired by the lateral inhibition patterns of orientation-tuned neurons in visual cortex. We normalize the response of each of the oriented filters with the average of all of them:

$$O_i'(x,y) = \left[O_i(x,y) - \frac{1}{N}\sum_{j=1}^{N} O_j(x,y) \right]_+ \qquad (2)$$

where $O_i(x,y)$ denotes the response of the ith orientation filter ($1 \le i \le N$) at position (x,y), and $O_i'(x,y)$ is the normalized filter response (here, $N = 4$). This across-orientation normalization leads to a clear improvement in detecting faint elongated objects (fig. 3d).

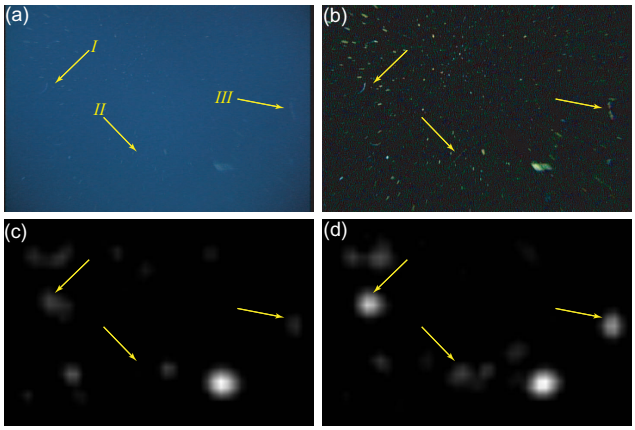

Figure 3: Example for the detection of faint elongated objects using across-orientation normalization. (a) original video frame with three faint, elongated objects marked; (b) the frame after background subtraction according to eq. 1 (contrast enhanced for displaying purpose); (c) the orientation conspicuity map (sum of all orientation feature maps) without across-orientation normalization; (d) the same map with across-orientation normalization. Objects I and III have a very weak representation in the map *without* normalization (c), and object II is not represented at all. The activation to the right of the arrow tip belonging to object II in (c) is due to a marine snow particle next to the object, and not due to object II. Compare with (d), where object II as well as the marine snow particle create activation. In the map *with* normalization (d), all three objects have a representation that is sufficient for detection.

2.3. Tracking

Once objects are detected, we extract their outline and track their centroid across the image plane using separate linear Kalman filters to estimate their x and y coordinates.

During QVTs the ROV is driven through the water column at a constant speed. While there are some animals that propel themselves with a speed that is comparable to or faster than the speed of the ROV, most objects either float in the water passively, or they move on a much slower time scale than the ROV. Hence it is justified to approximate that the camera is moving at a constant speed through a group of stationary objects.

Fig. 4 illustrates the geometry of the problem in the reference frame of the camera. In this reference frame, the object is moving at a constant speed in the x and z directions. The x coordinate of the projection onto the camera plane is:

$$x'(t) = \frac{x(t)\cdot z_c}{z(t)} = \frac{v_x z_c \cdot t + c_x z_c}{v_z \cdot t + c_z} \qquad (3)$$

To a second order approximation, the dynamics of this system can be described by a model that assumes constant acceleration:

$$\frac{d\underline{x}}{dt} = \begin{bmatrix} 0 & 1 & 0 \\ 0 & 0 & 1 \\ 0 & 0 & 0 \end{bmatrix} \underline{x} \qquad (4)$$

with the state vector $\underline{x}$ containing the projection coordinate x', its velocity v, and its acceleration a:

$$\underline{x} = \begin{pmatrix} x' \\ v \\ a \end{pmatrix} \qquad (5)$$

The dynamics in 4 result in a fundamental matrix that relates the state $\underline{x}(t)$ to the state a short time interval τ later $\underline{x}(t+\tau)$:

$$\Phi(\tau) = \begin{bmatrix} 1 & \tau & \frac{\tau^2}{2} \\ 0 & 1 & \tau \\ 0 & 0 & 1 \end{bmatrix} \qquad (6)$$

$\Phi(\tau)$ is used to define a linear Kalman filter [10, 11]. The deviations of this simplified dynamics from the actual dynamics are interpreted as process noise Q. The resulting

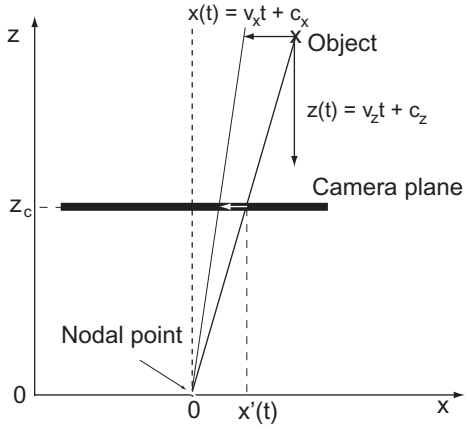

Figure 4: Geometry of the projection problem in the camera reference frame. The nodal point of the camera is at the origin, the camera plane is at z_c. The object appears to be moving at a constant speed into the x and z direction as the camera moves towards the object. Eq. 3 describes how the projection of the object onto the camera plane moves in time.

iterative equations for the Kalman filter are:

$$M_k = \Phi P_{k-1} \Phi^T + Q \quad (7)$$

$$K_k = M_k H^T \left(H M_k H^T + R \right)^{-1} \quad (8)$$

$$P_k = \left(I - K_k H \right) M_k \quad (9)$$

where P_0 is initialized to a diagonal matrix with large values on the diagonal, $R = [\sigma_m^2]$ is the variance of the measurement noise, $H = [1\ 0\ 0]$ is the measurement matrix, relating the measurement x^M to the state vector $\underline{x}$, and Q is the process noise matrix:

$$Q(\tau) = \sigma_p^2 \begin{bmatrix} \frac{1}{20}\tau^5 & \frac{1}{8}\tau^4 & \frac{1}{6}\tau^3 \\ \frac{1}{8}\tau^4 & \frac{1}{3}\tau^3 & \frac{1}{2}\tau^2 \\ \frac{1}{6}\tau^3 & \frac{1}{2}\tau^2 & \tau \end{bmatrix} \quad (10)$$

where σ_p^2 is the variance of the process noise. For our particular tracking problem we found $\sigma_m^2 = 0.01$ and $\sigma_p^2 = 10$ to be convenient values.

Once the Kalman matrix K_k is obtained from eq. 8, an estimation for $\underline{x}_k$ can be computed from the previous state estimate $\underline{\hat{x}}_{k-1}$ and the measurement x_k^M:

$$\underline{\hat{x}}_k = \Phi \underline{\hat{x}}_{k-1} + K_k (x_k^M - H \Phi \underline{\hat{x}}_{k-1}) \quad (11)$$

When no measurement is available, a prediction for $\underline{x}_k$ can be obtained by extrapolating from the previous estimate:

$$\underline{\hat{x}}_k = \Phi \underline{\hat{x}}_{k-1} \quad (12)$$

For the initiation of the tracker we set $\underline{\hat{x}}_0 = [x_0^M\ 0\ 0]^T$, where x_0^M is the coordinate of the object's centroid obtained from the saliency-based detection system described in the previous section.

We employ the same mechanism to track the y coordinate of the object in the camera plane. Whenever the x or the y coordinate tracker runs out of the camera frame, we consider the track finished and the corresponding object lost. Re-entry of objects into the camera frame almost never occurs in our application. We require that an object is successfully tracked over at least five frames, otherwise we discard the measurements as noise.

In general, multiple objects are tracked simultaneously. Usually, such multi-target tracking raises the problem of assigning measurements to the correct tracks [12]. Since the attention algorithm only selects the most salient objects, however, we obtain only a few objects whose predicted locations are usually separated far enough to avoid ambiguities. If ambiguities occur, they are resolved using a measure that takes into account the Euclidean distance of the detected objects from the predictions of the trackers, and the size ratio of the detected and the tracked objects.

2.4. Towards Classification

Ultimately, it is our goal to not only detect and track salient objects, but also to classify them into biological taxonomies. This may seem very difficult, given that currently on the order of 400 species and families are being annotated routinely. However, in a recent study [13] we determined that in the human annotations between 1997 and 2002, the ten most common animals correspond to 60%, and the 25 most common animals to 80% of all annotations. Thus, if we succeed in recognizing the 25 most common animals reliably, we can automate many scientific missions that concentrate on those most abundant animals. To date, our experiments using low-level features such as major and minor axes, aspect ratio, total area size, maximum and average luminance over the shape of the object to classify detected objects into the broad categories "interesting" and "not interesting" are inconclusive. The classification into species remains an open issue for us.

2.5. Implementation

At MBARI, two ROVs are used for deep sea exploration, the ROV Ventana and the ROV Tiburon [14, 15]. ROV Ventana, launched from R/V Point Lobos, uses a Sony HDC-750 HDTV (1035i30, 1920x1035 pixels) camera for video data acquisition, and the data are recorded on a DVW-A500 Digital BetaCam video tape recorder (VTR) on board the R/V Point Lobos. ROV Tiburon operates from R/V Western Flyer; it uses a Panasonic WVE550 3-chip CCD (625i50, 752x582 pixels) camera, and video is also recorded on a DVW-A500 Digital BetaCam VTR. On shore, a Matrox RT.X10 and a Pinnacle Targa 3000 Serial Digital Interface

video editing card in a Pentium P4 1.7 GHz personal computer (PC) running the Windows 2000 operating system and Adobe Premier are used to capture the video as AVI or QuickTime movie files at a resolution of 720 x 480 pixels and 30 frames per second. The frames are then converted to Netpbm color images and processed with our custom software.

All software development is done in C++ under Linux. To be able to cope with the large amount of video data that needs to be processed in a reasonable amount of time, we have deployed a computer cluster with 8 Rack Saver rs1100 dual Xeon 2.4 GHz servers, configured as a 16 CPU, 1 Gigabit Ethernet Beowulf cluster. We currently process approximately three frames per second on each of the Xeon nodes at a resolution of 720x480 pixels. We are optimistic that additional hardware and software optimization will enable us to process 30 frames per second in real time soon.

For example videos before and after processing with our system see our project web page http://www.mbari.org/AVED or the supplementary material for this paper.

3. Results

We present two groups of results – an assessment of the attenional selection algorithm for our purpose, and a comparison of a processed 10 min video clip with expert annotations.

3.1. Single frame results

In order to assess the suitability of the saliency-based detection of animals in video frames in the early stage of our project, we analyzed a few hundred single video frames. We captured the images at random from a typical video stream. We did this analysis for two image sets – one with 456 images from video recorded by ROV Tiburon on June 10, 2002, and one with 1004 images from video recorded by ROV Ventana on June 18, 2002. Only some of the images in the two sets contain animals. To evaluate the performance of the attentional detection system described in section 2.2 for this application domain, we counted in how many of the images the most salient location, i.e. the location first attended to by the algorithm, coincides with an animal. The results are displayed in table 1.

In the images that did not contain animals, the saliency mechanism identified other visual features as being the most salient ones, usually particles of marine snow. For the majority of the images that did contain animals, the saliency program identified the animal (or one of the animals, if more than one were present) as the most salient location in the image. In image set 1, the animals were identified as the most salient objects in 89% of all images that contained animals. In image set 2 this was the case for 88% of the images with animals. Ground truth was established by individual inspection of the test images.

Table 1: Single frame analysis results.

	Image set 1	Image set 2
Date of the dive	06/10/2002	06/18/2002
ROV used for the dive	Tiburon	Ventana
Number of images obtained	456	1004
Images without animals	205	673
Images with detected animals	224	291
Images with missed animals	27	40

3.2. Video processing

As a test of the video processing capabilities of our system, we processed a 10 min video segment that had been annotated by scientists before. The scientists annotated 57 object in this video clip. Our system detected 40 of those. In two cases, our automated detection system detected animals that the annotators had missed. The program also detected several other objects (mostly debris) that the scientists had not annotated. However, we do not consider these cases to be false positives, because a classification system capable of recognizing species would also be able to distinguish target animals from salient debris.

Table 2: Missed species.

Annotation	# of misses	Remark
Nanomia	14	sub-class Siphonophora
Siphonophora	1	faint, string-like animal
Calycophora	1	sub-class Siphonophora
Solmissus	1	Narcomedusa: small jellyfish

Our system missed 17 of the 57 annotated objects in the video clip. Table 2 shows details about the species that were missed. As can be seen, almost all misses are of the subclass Siphonophora, which are long string-like colonial animals that yield very low contrast in the video frames.

In a more recent set of experiments we obtained very similar results. In three video sequences, a total of 167 (80%) of 208 human-annotated animals were detected successfully, 41 (20%) were missed, and 22 animals were found by our software that the human annotator had missed. Again, many misses (19 out of 41) are siphonophores.

The difficulty of detecting these animals even for humans is illustrated by the fact that 13 of the 22 animals missed by the human annotator but found by the software are siphonophores as well. In further improvements of the system we plan to specifically address detection of these objects in the video stream.

4. Conclusion

We present a new method for processing video streams from ROVs automatically. This technology has potentially significant impact on the daily work of video annotators by aiding their analysis of noteworthy objects in the videos. After continued refinement, we hope that the software will be able to perform a number of routine tasks fully automatically, such as "outlining" video, analyzing QVT videos for the abundance of certain easily identifiable animals, and marking especially interesting episodes in the videos that require the attention of an expert annotator.

Beyond its applications to ROV videos, our method for automated underwater video analysis has potential for enabling Autonomous Underwater Vehicles (AUVs) to collect and analyze QVTs. AUVs could sample more frequently and at an ecologically significant finer spatial resolution and greater spatial range than is practical and economical for ROVs [16]. We also see great benefit in automating portions of the analysis of video from fixed observatory cameras, where autonomous response to potential events (e.g. pan and zoom to tracked objects), and automated processing for science users of potentially very sparse video streams from 100s of network cameras could be key to those cameras being practical scientific instruments.

We have shown previously that attentional selection algorithms can successfully cue object recognition systems for learning and recognition of multiple objects [7, 17]. In our present study we demonstrate the use of such an algorithm for multi-target tracking. In particular, the saliency-based attention system detects the targets for track initiation, and it decreases the complexity of the assignment problem in multi-target tracking by selecting only the most relevant targets. This integration of techniques makes the automation of our underwater tracking problem feasible.

Acknowledgments

This project originated at the 2002 Workshop for Neuromorphic Engineering in Telluride, CO, USA. We thank the David and Lucille Packard Foundation, NSF, NIMH and the NSF Research Coordination Network (RCN) Institute for Neuromorphic Engineering (INE) for making this research possible. We thank K. Salamy, J. Harmssen and A. Wilson for technical assistance at MBARI. M. Risi engineered our video capture system, D. Cline engineered the Beowulf computer cluster, and R. Sherlock guided our analysis of video images. We thank B. Robison, J. Connor, N. Jacobsen Stout and the MBARI video lab staff for their interest and support.

References

[1] T. Clarke. Robots in the deep. *Nature*, 421(30):468–470, 2003.

[2] B.H. Robison. The coevolution of undersea vehicles and deep-sea research. *Marine Technology Society Journal*, 33:69–73, 2000.

[3] B.H. Robison, K.R. Reisenbichler, R.E. Sherlock, J.M.B. Silguero, and F.P. Chavez. Seasonal abundance of the siphonophore, Nanomia bijuga, in Monterey Bay. *Deep-Sea Research II*, 45:17411752, 1998.

[4] J.M.B. Silguero and B.H. Robison. Seasonal abundance and vertical distribution of mesopelagic Calycophoran siphonophores in Monterey Bay, CA. *Journal of Plankton Research*, 22:1139–1153, 2000.

[5] L. Itti, C. Koch, and E. Niebur. A model of saliency-based visual attention for rapid scene analysis. *IEEE PAMI*, 20(11):1254–1259, 1998.

[6] L. Itti and C. Koch. Target detection using saliency-based attention. In *Proc. RTO/SCI-12 Workshop on Search and Target Acquisition (NATO Unclassified)*, pages 3.1–3.10, Utrecht, The Netherlands, 1999.

[7] U. Rutishauser, D. Walther, C. Koch, and P. Perona. Is attention useful for object recognition? In *CVPR*, 2004.

[8] E.P. Simoncelli and W.T. Freeman. The steerable pyramid: a flexible architecture for multi-scale derivative computation. In *ICIP*, 1995.

[9] R. Manduchi, P. Perona, and D. Shy. Efficient implementation of deformable filter banks. *IEEE Transactions on Signal Processing*, 46(4):1168–1173, 1998.

[10] R.E. Kalman and R.S. Bucy. New results in linear filtering and prediction theory. *Journal of Basic Engineering*, 83(3):95–108, 1961.

[11] P. Zarchan and H. Musoff. *Fundamentals of Kalman filtering: a practical approach*. Progress in astronautics and aeronautics. American Institute of Aeronautics and Astronautics, Inc., 2000.

[12] T. Kirubarajan, Y. Bar-Shalom, and K.R. Pattipati. Multiassignment for tracking a large number of overlapping objects. *IEEE TAES*, 37(1):2–21, 2001.

[13] A. Wilson and D.E. Edgington. First steps towards autonomous recognition of Monterey Bay's most common mid-water organisms: Mining the ROV video database on behalf of the Automated Visual Event Detection (AVED) system. Technical report, MBARI, 2003.

[14] J. B. Newman and D. Stakes. Tiburon, development of an ROV for ocean science research. In *Proceedings MTS/IEEE Oceans*, Brest, France, 1994.

[15] E. Mellinger, A. Pearce, and M. Chaffey. Distributed multiplexers for an ROV control and data system. In *Proceedings MTS/IEEE Oceans*, Brest, France, 1994.

[16] K. Smith. NEPTUNE science white paper #6: Deep-sea ecology. `http://www.neptune.washington.edu/science_wrkgp/127_deep_sea_final.html`, June 18 2002.

[17] D. Walther, L. Itti, M. Riesenhuber, T. Poggio, and C. Koch. Attentional selection for object recognition – a gentle way. In *Biologically Motivated Computer Vision*, pages 472–479, 2002.